Universiteit Antwerpen

This item is the archived peer-reviewed author-version of:

Fast spatial-selective delivery into live cells

Reference:

Xiong Ranhua, Drullion Claire, Verstraelen Peter, Demeester Jo, Skirtach Andre G., Abbadie Corinne, De Vos Winnok, De Smedt Stefaan C., Braeckmans Kevin.- Fast spatial-selective delivery into live cells
Journal of controlled release - ISSN 0168-3659 - 266(2017), p. 198-204
Full text (Publisher's DOI): https://doi.org/10.1016/J.JCONREL.2017.09.033
To cite this reference: http://hdl.handle.net/10067/1455880151162165141

uantwerpen.be
Institutional repository IRUA

ACCEPTED MANUSCRIPT

Fast spatial-selective delivery into live cells

Ranhua Xiong[1,2], Claire Drullion[3], Peter Verstraelen[4], Jo Demeester[1], Andre G. Skirtach[2,5], Corinne Abbadie[3], Winnok H. De Vos[2,4,5], Stefaan C. De Smedt[1,6], Kevin Braeckmans[1,2,7,8*]

[1]Laboratory of General Biochemistry and Physical Pharmacy, Faculty of Pharmaceutical Sciences, Ghent University, 9000 Ghent, Belgium

[2]Centre for Nano- and Biophotonics, Faculty of Pharmaceutical Sciences, Ghent University, 9000 Ghent, Belgium

[3]Univ. Lille, CNRS, Institut Pasteur de Lille, UMR 8161 – M3T - Mechanisms of Tumorigenesis and Targeted Therapies, 59000 Lille, France

[4]Department of Veterinary Sciences, University of Antwerp, 2020 Antwerp, Belgium

[5]Department of Molecular Biotechnology, Ghent University, 9000 Ghent, Belgium

[6]College of Chemical Engineering, Jiangsu Key Lab of Biomass-based Green Fuels and Chemicals, Nanjing Forestry University (NFU), Nanjing, 210037 PR China

[7]Univ Lille 1, Univ Lille Nord France, IEMN, UMR 8520, 59652 Villeneuve D'Ascq, France

[8]Univ Lille 1, Univ Lille Nord France, Lab Phys Lasers Atomes & Mol, UMR 8523, 59655 Villeneuve D'Ascq, France

***Tel** : +32 9 264 80 98

***Fax** : +32 9 264 81 89

***E-mail**: Kevin.Braeckmans@UGent.be

ACCEPTED MANUSCRIPT

ACCEPTED MANUSCRIPT

Abstract

Intracellular delivery of functional compounds into living cells is of great importance for cell biology as well as therapeutic applications. Often it is sufficient that the compound of interest (being a molecule or nanoparticle) is delivered to the cell population as a whole. However, there are applications that would benefit considerably from the possibility of delivering a compound to a certain subpopulation of cells, or even in selected single cells. Here we report on an integrated platform for high-throughput spatially resolved nanoparticle-enhanced photoporation (SNAP) of adherent cells. SNAP enables safe, intracellular delivery of exogenously administered nanomaterials in selected subpopulations of cells, even down to the single cell level. We demonstrate the power of SNAP by selectively delivering a safe contrast agent into a subpopulation of polynucleated keratinocytes, enabling their downstream purification for unraveling their role in neoplasm formation. The flexibility and speed with which individual cells can be labeled make SNAP an ideal tool for high-throughput applications, not only for selective labeling but also for targeted drug delivery.

Keywords: Intracellular delivery, cell-selective delivery, nanoparticles, pulsed laser, vapor nanobubbles

ACCEPTED MANUSCRIPT

ACCEPTED MANUSCRIPT

Introduction

Intracellular delivery of functional compounds into living cells is of great importance for e.g. cellular imaging[1, 2], therapy[3] and fundamental cell-biology research[4, 5]. For many applications it is sufficient that the compound of interest (being a molecule or nanoparticle) is delivered to the cell population as a whole, for which there are variety of delivery methods, such as lipofection or electroporation[6]. However, there are other applications that would benefit considerably from the possibility of delivering a compound to a certain subpopulation of cells, or even in single cells. For example, delivery of nucleic acids into single cell results in single-cell resolution of gene expression which is beneficial to elucidate gene functions[7]. Cell-selective delivery is also of interest when working with heterogeneous cell cultures. Phenotypic and genomic heterogeneity in a cell population leads to inaccuracy and obscuration of cell differentiation when the population is analyzed as a whole. Delivering e.g. inhibitors into individual target cells and analyzing the outcome at the single-cell level allows to accurately regulate and resolve changes in differentiation at the single-cell level[8].

Methods which allow fast and flexible cell-selective intracellular delivery of molecules or nanoparticles are, however, scarce. Microinjection could serve this purpose, but is technically demanding and not amenable to upscaling[9]. Spatially resolved electroporation has been explored as well[10, 11], demonstrating that cells could be selectively transfected by an array of microelectrodes. This method is, however, limited by the fact that transfections are only possible according to the pre-defined layout and size of the electrodes, which, for instance, would not allow transfecting one single cell in a (co-) culture. Photoporation offers a valuable alternative approach to deliver compounds to cells in a targeted manner. Here, selected cells are transiently permeabilized at a particular location of the cell membrane with a precisely focused laser beam[12, 13]. Particular benefits of this approach are that it is a contact free method (as opposed to microinjection) and that the laser beam can be precisely controlled to target any cell[12-14]. While this method was successfully applied to single cell transfections with DNA, or mRNA[12, 13], it remains limited in throughput. In a fully automated device with a specially engineered laser beam only a few cells per second could be photoporated[14]. Photoporation throughput can be tremendously sensitized by making

ACCEPTED MANUSCRIPT

use of plasmonic nanoparticles (NPs), like gold nanoparticles (AuNPs), that have a large absorption cross section[15], and are known to raise temperature upon suitable laser irradiation[16]. When adsorbed to the cell membranes they can permeabilize the cell membrane upon laser irradiation through distinct thermally induced phenomena such as local heating, acoustic shockwaves, or the formation of disruptive water vapour nanobubbles (VNB)[17]. NP sensitized photoporation can offer higher throughput since less laser energy density is needed so that the laser beam can be expanded to irradiate tens or even hundreds of cells at the same time. NP sensitized photoporation has proven to be fast (>1000 cells/s)[18] and efficient at delivering a broad variety of molecules into cells, such as siRNA, pDNA, and proteins[4, 17, 18].

Based on these distinct advantages, here we aimed to explore the unexploited potential of nanoparticle-sensitized photoporation to safely (*i.e.*, in a non-cytotoxic manner) deliver compounds into precisely selected subpopulations of cells, in high-throughput and with great flexibility. To this end we developed Spatially-resolved NAnoparticle-sensitized Photoporation (SNAP) and implemented this technology according to two different operational modes. In the first mode, cells are selectively photoporated according to a pre-defined pattern, which is useful for experiments where the location rather than the cell type is of importance (**Fig. 1b, c**). In the second mode, cells are photoporated in an image-guided interactive way, where microscopy images are used to (automatically) select the cells of interest (**Fig. 1d, e**). We start with a detailed description and characterization of the various SNAP modes, after which we demonstrate the flexibility of this new enabling technology to a challenging example application. We explore SNAP to selectively label morphologically distinct primary normal human epidermal keratinocytes (NHEKs). In particular, polynucleated or mononucleated NHEKs are separately labeled so that they can be isolated for further downstream molecular and functional analysis in relation to cancer research.

Results and discussion

The first step in SNAP is to incubate cells with plasmonic nanoparticles (see **Fig. 1a**). In this work we have used cationic 70 nm AuNPs which easily adsorb to the cell membrane. After 30 min incubation, cells are typically washed to remove unbound AuNPs, leaving

ACCEPTED MANUSCRIPT

between 5 and 10 AuNP associated per cell, as can be verified with confocal reflection microscopy (**Fig. S1a**). The average number of AuNPs associated to cells can easily be controlled by adjusting the AuNP concentration that is added to the cells as reported before [17]. A higher concentration of AuNP will lead to more VNB and thus more pores in the cell membrane. While this allows more compound to enter into cells, it also leads to increased cell toxicity. Therefore, the concentration used here was optimized to obtain as much as possible intracellular delivery while keeping toxicity at a minimum (i.e. cell viability at least 80%). The next step is to add the compound of interest into the cell medium, followed by laser irradiation. Here we made use of vapour nanobubble (VNB) photoporation as it has been shown before to be a very efficient cell permeabilization mechanism. Briefly, upon absorption of a laser pulse (7 ns) with a fluence above the VNB threshold (here we used 2 J/cm^2 as optimized before[17, 19]) the AuNP's temperature increases sufficiently to let the surrounding water evaporate. This results in the formation of VNBs that expand and collapse, inducing nanopores in the cell membrane and allowing the compound of interest to diffuse into the cell cytoplasm. The pores have a size up to about hundreds of nanometers and recover in a 1-3 min time frame, as reported before. As shown in **Fig. S1b** and **Movie S1**, only irradiated cells become photoporated, in this case with Propidium Iodide (PI). In our set-up the diameter of the photoporation laser beam can be adjusted so that either single or multiple cells can be irradiated per laser pulse. A programmed motorized microscope stage is used to move the sample with respect to the laser beam (see **Fig. S2** and **Methods**) so as to photoporate the cells of interest. SNAP was implemented according to two distinct modes: photoporation according to a pre-defined spatial pattern or in an interactive image-guided manner (**Fig. 1b-e**). Each mode can be used in two ways, as will be explained in detail below.

ACCEPTED MANUSCRIPT

ACCEPTED MANUSCRIPT

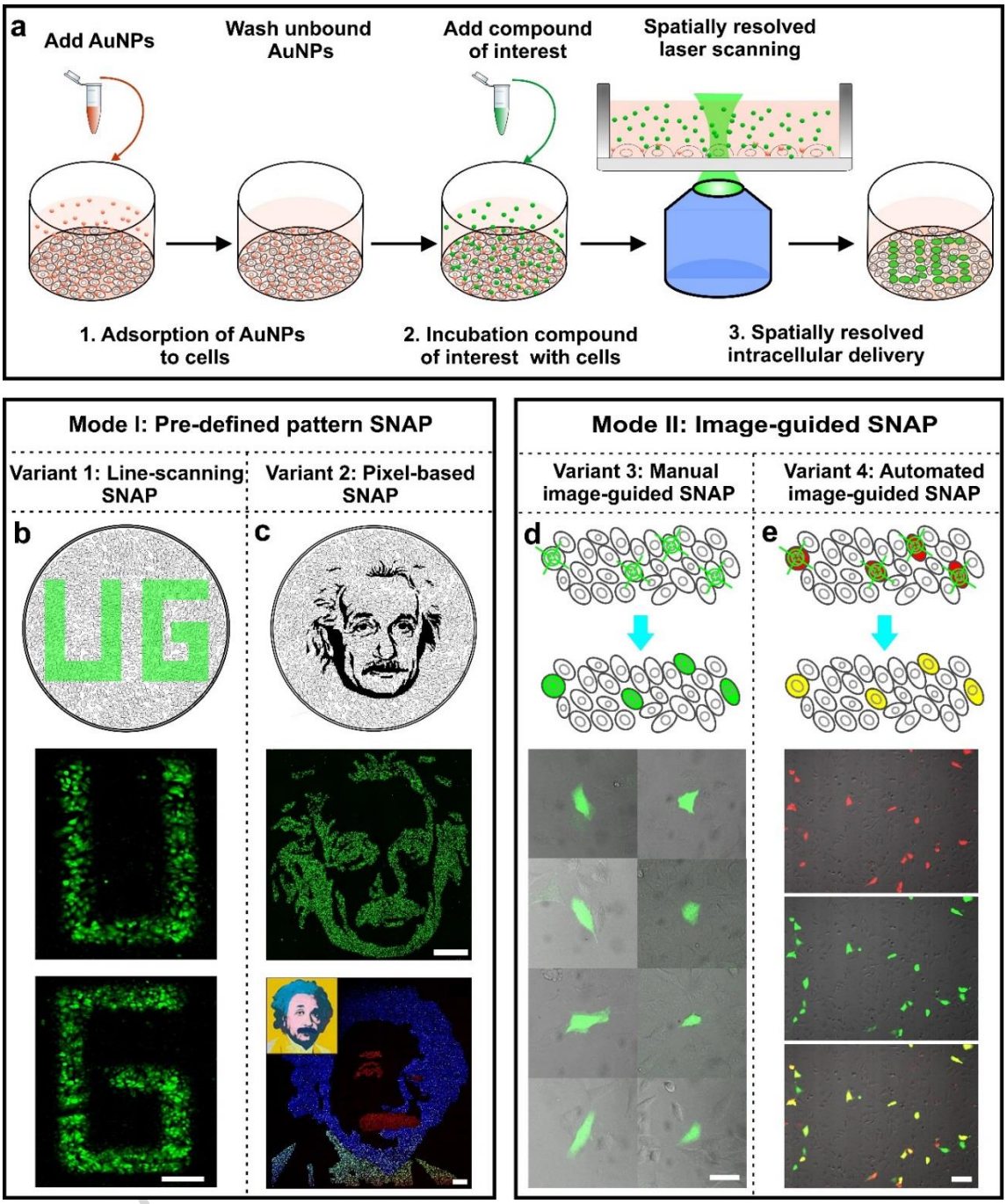

Figure 1. Schematic overview of SNAP. (**a**) Following AuNP incubation and washing of unbound AuNPs, the compound that should be delivered into the cells is added to the cell medium. An automated xy-stage is used to perform photoporation in selected areas of the cell culture. Only those cells that receive a laser pulse will be photoporated and take up the compound that was added to the medium, while the other cells remain unaffected. (**b**) By line-scanning of the sample through the photoporation laser beam, HeLa cells were photoporated with quantum dots (QDs) forming the letters 'U' and 'G' in the cell culture. Scale bar is 150 µm. (**c**) In the pixel-based variant the photoporation beam is directed towards distinct locations

ACCEPTED MANUSCRIPT

in the cell culture according to the pixels of a binary image. HeLa cells were photoporated with FITC-dextran with 10 kDa (FD10) according to the black pixels of a drawing of Albert Einstein. By repeating the photoporation procedure it is possible to deliver different compounds to different regions in the cell culture. As an example, Andy Warhol's painting of Einstein was reproduced by photoporating HeLa cells sequentially with cascade blue-dextran (blue), FITC-dextran (green) and Alexa 647-dextran (red). Scale bars are 1000 µm. (**d**) Image-guided cell-selective photoporation is possible by first recording microscopy images of the cell culture. The user can then select manually which cells are of interest and should become photoporated. Here, selected HeLa cells were photoporated with FD10 (green), demonstrating that single cell precision can be achieved. Scale bar is 50 µm. (**e**) The entire process can be automated if cell selection is done by automated image analysis. Cells of interest may be identified based on morphological features or, as in this example, based on a fluorescent cell marker. Red-labeled HeLa cells were mixed with unlabeled ones in a ratio of 1:5 and automatically localized by image processing for subsequent photoporation with FD10 (green). Scale bar is 100 µm.

Pre-defined pattern SNAP

The simplest way to perform SNAP according to a pre-defined pattern is by 'line scanning'. Cells can be photoporated according to simple geometrical shapes by scanning the sample line-by-line through the laser beam, as schematically shown in **Fig. S3a**. One example is shown in **Fig. 1b** where HeLa cells were photoporated with quantum dots (QDs). Note that the line width is simply determined by the (adjustable) diameter of the photoporation laser beam. Indeed, as shown in **Fig. S3b**, changing the diameter of the laser beam also changes the width of the photoporated lines of cells. With a laser beam of 150 µm and a pulse repetition rate of 20 Hz the stage can move at 3 mm/s, which corresponds to a photoporation rate of about 200 cells/s. Evidently, if a laser with higher pulse repetition rate is used, even higher photoporation rates are possible.

If more complex patterns are desired, a 'pixel-based' approach is more convenient where the photoporation pattern is defined in a binary image. As illustrated in **Fig. S3c**, a single laser pulse is applied to the sample according to the black pixels in the binary image. At each of those pixel locations a single laser pulse is applied to locally photoporate the cells. The mapping of the image to the cell culture is done such that one image pixel corresponds to 80% of the laser beam diameter. This ensures a small spatial overlap between subsequent photoporation pulses so that all cells in the selected area are effectively photoporated. An example is shown in **Fig. 1c** where HeLa cells were

ACCEPTED MANUSCRIPT

photoporated with FITC-dextran of 10 kDa (FD10) according to a black-and-white drawing. The zoomed-in images in **Fig. S4** clearly show the individually labeled cells. By sequential repetitions of the procedure it is even possible to delivery different compounds into different regions of the cell culture. An example is given in **Fig. 1c** and **Movie S2** where three rounds of photoporation were subsequently performed with cascade blue-dextran, Alexa 647-dextran and FITC-dextran. Another example is shown in **Fig. S5** and **Movie S3** where 6 colors were used. Compared to a previous report where a simple pattern of region or letters was created by means of a pre-fabricated light-absorption or light-obstructing mask [20, 21], the scanning approach by SNAP is of course much more flexible allowing any pattern to be created simply by using a binary image of choice.

Image-guided SNAP

While photoporation according to pre-defined patterns can be useful for some applications such as the study of cell migration or bystander effects, many other applications would rather benefit from photoporating certain subtypes of cells which do not necessarily have a fixed location in the culture. Such cells could be identified based on distinctive features like cell or nuclear morphology, or the presence of a certain (fluorescent) biomarker. Therefore, as a next step, we implemented image-guided photoporation of selected cells with both a manual (**Fig. 1d**) and automated (**Fig. 1e**) cell recognition mode of operation. In the manual mode, the user indicates in prerecorded microscopy images which cells should be photoporated. As shown in **Fig. 1d**, single cell resolution is easily obtained when reducing the photoporation laser beam diameter to slightly less than the size of a typical cell. Cells can also be automatically selected by integrating automated image analysis in the pipeline. A proof-of-concept is shown in **Fig. 1e** where the cells of interest have a red fluorescent reporter signal. This sample was obtained by first photoporating HeLa cells with Alexa 647-dextran (AD), after which these cells were trypsinized and reseeded with unlabeled HeLa cells at a 1:5 ratio. The cell culture was imaged by fluorescence microscopy and the red labeled cells were localized by a simple image processing procedure (**Fig. S6**). Subsequently, SNAP was carried out to deliver green fluorescent FD10 into those cells (**Fig. 1e** and **Fig. S7a, b**). Colocalization analysis revealed that 70.4 ± 9.7% (n=3) of the red-fluorescent targeted cells were successfully labeled with FD10. About 30% of the cells were incorrectly

ACCEPTED MANUSCRIPT

labeled with FD10. These false positive cells are on the one hand due to a small amount of dead cells into which FD10 can diffuse. On the other hand, false positives also arise from inaccurate positioning of the photoporation laser beam, which is due to two reasons. First, the relatively simple image processing method that we have used to identify the cell's position (based on the maximum intensity) in some cases doesn't indicate the exact center of the cell. Secondly, cells sometimes move or divide between taking the images and the actual photoporation procedure so that they are not exactly at the indicated position anymore. In next generations of the SNAP technology these two shortcomings can be addressed by improving the cell detection algorithm and by integrating SNAP with confocal microscopy to minimize the time delay between imaging and photoporation. It is of note that these false positives can be reduced by a subsequent targeted photobleaching procedure (**Fig. S7c**). After two rounds of photobleaching the false positive cells could be reduced to 5% (**Fig. S7d**). The photoporation throughput in the image-guided mode is slower as for the pre-defined patterns as per laser pulse only one cell can be photoporated. With our current 20 Hz laser this means that the photoporation rate was limited to 20 cells/s, which is still an order of magnitude more than the highest reported rate for standard photoporation. Higher photoporation rates are very well possible if a laser with higher pulse frequency is used.

ACCEPTED MANUSCRIPT

ACCEPTED MANUSCRIPT

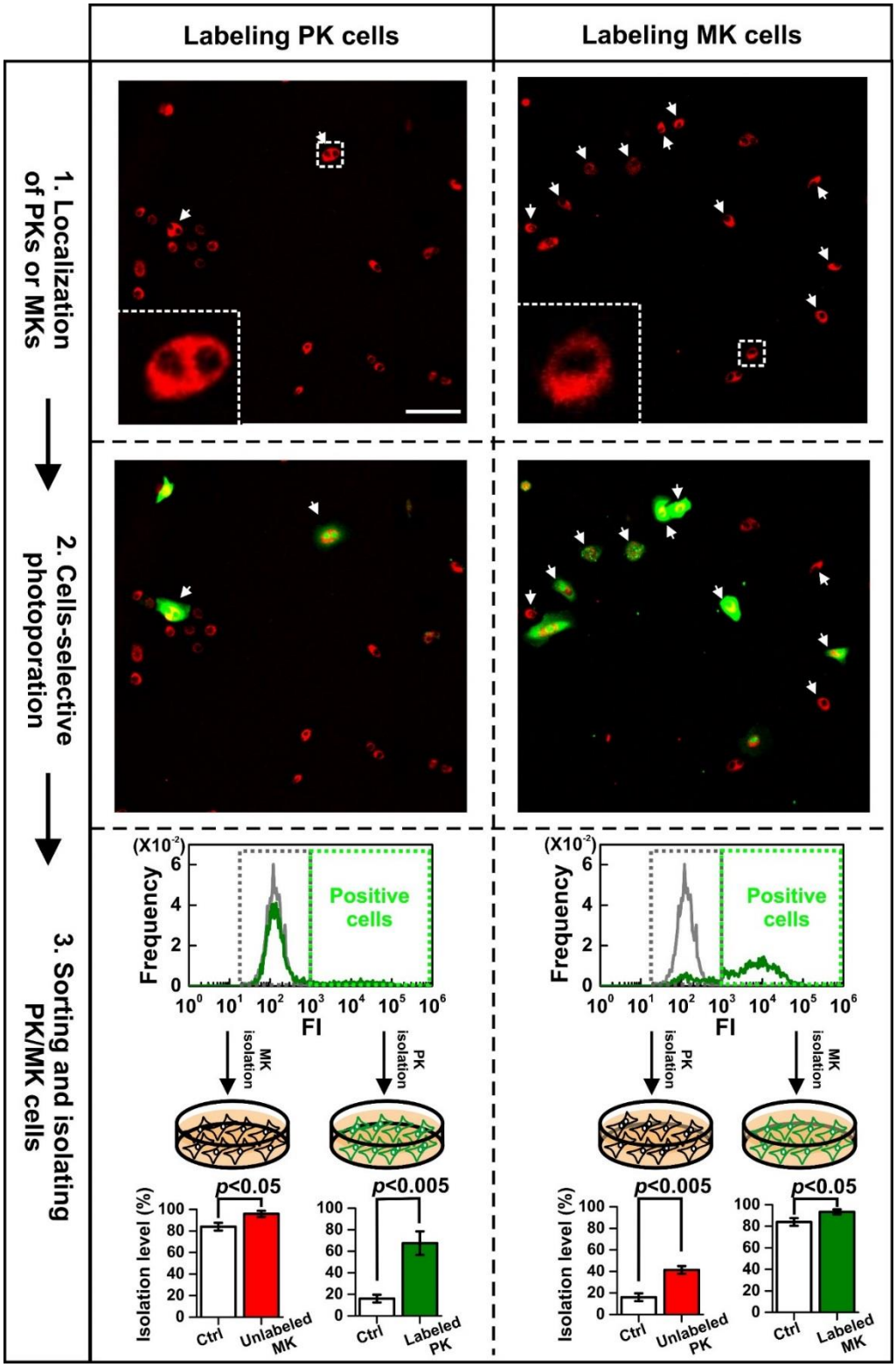

Figure 2. SNAP enables non-toxic isolation of mononuclear and polynuclear NHEKs. Endolysosomes in the perinuclear area are labeled by 24 h incubation of NHEKs with 10 kDa Alexa 647-dextran (red). Following the identification of mononuclear NHEKs (MK) and polynuclear NHEKs (PK) by automated

ACCEPTED MANUSCRIPT

image processing (indicated by white arrows), either of both populations is selectively labeled with FD10 (green) by automated image-guided SNAP. Separation and isolation of both populations is finally done by FACS after trypsinisation of the cells. Cell frequency (n=5000) vs. fluorescence intensity (FI) is shown for photoporated (green) and control (grey) cells. The percentage of PK and MK cells are shown before (white bars) and after (green and red bars) isolation. The results are the mean ± SD of n=3 independent biological repeats. The data are compared with ANOVA test. Scale bar is 100 µm.

As an example application, SNAP was used to enable the isolation of morphologically distinct subpopulations of cells in culture. In particular, we aimed to isolate relatively rare polynucleated from mononucleated primary normal human epidermal keratinocytes (NHEKs). In contrast to cancerous cells, normal diploid cells cannot divide indefinitely, but rather enter a senescent state after a finite number of divisions. While senescence is characterized by an irreversible cell cycle arrest, several studies indicate that this state may not be as stable as generally assumed[22]. Some senescent cells could re-renter the cell cycle and generate precancerous daughter cells, called post-senescence neoplastic emergent (PSNE) cells that are mutated, transformed and tumorigenic[22, 23] (**Fig. S8**). Based on microscopy observations it has been suggested that polynucleated senescent cells are the progenitors of PSNE cells. In order to study this important phenomenon in more detail, it is of current interest to isolate polynuclear keratinocytes (PKs) from mononuclear keratinocytes (MKs) in a non-toxic manner to enable further downstream molecular and functional analyses. Initial attempts to sort polynuclear cells with FACS using a cell-permeable nuclear stain like Hoechst, failed due to substantial long-term toxicity, with only 37.2 ±11.9% (n=3) cells surviving after 4 days measured by MTT. Hence we explored if SNAP could be used to selectively label one of both subpopulations with an inert non-toxic fluorescent probe (FD10) that would not cause long-term cytotoxicity. For easy cell identification, we first incubated the cells with 10 kDa Alexa 647-dextran (AD) for 24 h, which labels the late endosomes and endo-lysosomes in the perinuclear area. At low magnification the nuclei are then visible as dark areas, as can be seen in **Fig. 2**. Contrary to Hoechst staining, this type of labeling was found to be completely harmless to NHEKs with 103.7% ± 9.7 cells surviving after 4 days. An image processing protocol was designed to automatically locate either PK or MK cells, as outlined in **Fig. S9**. These locations were then used to deliver FD10 to the targeted

ACCEPTED MANUSCRIPT

subpopulation by automated image-guided SNAP (**Fig. 2**). An AuNP concentration of 2.5×10^7 nps/ml and a laser fluence of 1.0 J/cm^2 were chosen for the photoporation experiments on NHEKs because under these conditions we achieved >90% labeling efficiency with ~80% cell viability (**Fig. S10**). When targeting PK cells we found that 67.1 ± 9.5% (n=3) the labeled cells were actually PK cells, which is close to the expected ~70% accuracy that we found earlier for HeLa cells. When targeting MK cells we achieved an accuracy of 95.9 ± 3.2% (n=3). This higher value can be explained by the fact that most of the cells are MKs so that upon mistargeting it is very likely that still a MK is being photoporated. In a next step we tried isolating MK from PK by FACS sorting. Based on visual inspection the initial cell culture consisted of 17% polynuclear cells and 83% mononuclear cells. When sorting was done based on labeled PK cells, PK cells could be purified to 65%, which is 4 fold higher than the initial culture (see left panel, **Fig. 2**). At the same time the purity of MK cells increased to 93%. When cells were sorted based on labeled MK cells, the PK purity could be improved from 17% to 40%, while MK purity increased from 83% to >95%. These results show that the best enrichment of a particular subpopulation is achieved when that particular fraction is labeled. In case, however, one would want to avoid introducing a label into the cells that are of interest for further downstream analysis, the results show that enrichment of a particular subpopulation is still possible by labeling the other fraction of cells, although at a lower efficiency. Finally we would like to note that higher purification levels could evidently be reached by simple repetition of the entire procedure (and optimization of the SNAP technology as already pointed out above). Taken together we conclude that automated image-guided SNAP succeeded in isolating for the first time PK cells from MK cells without inducing long-term toxicity. This will be very helpful in further research aimed at determining the molecular specificities of PK cells that confer the ability to escape from senescence and generate mutated daughter cells.

Conclusions

In summary, we have developed a methodology that can be used to deliver molecules such as fluorescent labels into living cells in a spatially resolved manner with great flexibility and in high throughput, even down to single cell resolution. Spatial selective

ACCEPTED MANUSCRIPT

delivery can be performed according to pre-defined patterns or in an interactive image-guide manner. By full automation of the procedure we achieved delivery rates that exceed the fastest reported methods by more than one order of magnitude[12-14]. We expect that speed can be increased by at least another order of magnitude when using a laser with higher pulse frequency. Interestingly, spatial selective delivery with single cell resolution was recently also demonstrated with a planar arrangement of laser-illuminated gold nanotubes on top of which cells are grown[24]. Throughput was, however, very low as cells had to be manually positioned into the laser beam. In addition, such an approach requires specially microfabricated substrates and is inherently limited to 2-D cell cultures. Instead, SNAP is compatible with normal microscopy samples and may be extended to 3-D cell cultures as well. While we showed one application where cells were selectively labeled with contrast agents, our platform is equally suited to deliver biologically active molecules, such as smaller nucleic acids or proteins, into selected cells. Indeed, based on our previous work molecules with a hydrodynamic size of up to 20-30 nm could be fairly easily delivered into cells[19]. This could, for instance, be of interest to enable spatially controlled differentiation of stem cells for tissue engineering[25].

ACCEPTED MANUSCRIPT

ACCEPTED MANUSCRIPT

Materials and Methods

Materials. Cationic AuNPs of 70 nm were purchased from NanoPartz (#CU11-70-P30-50, Nanopartz Inc., Loveland, CO, USA).). According to the manufacturer the AuNP had a size of 70 nm and a zeta potential of +30 mV. 520 (±10) nm CdSe/ZnS QD coated with a thiol oligomer and surface functionalized with -COOH groups (PEG-coated QDs) were purchased from Mesolight, Inc. (#CdSe/ZnS-PEG-COOH-520, Mesolight, Inc., Little Rock Arkansas, USA). FITC-dextrans with a molecular weight of 10 kDa were purchased from Sigma-Aldrich (Belgium). Cascade Blue dextran (#D-1976, Molecular Probes^{TM}), Alexa@647 labelled dextran 10 kDa (#D-22914, Molecular Probes^{TM}), and Propidium Iodide (#P1304MP, Molecular Probes^{TM}) were purchased from Invitrogen (Belgium).

Platform for SNAP. The photoporation platform consists of a custom developed setup that includes optical and electrical components to generate and detect vapour nanobubbles (VNB). The set-up is built around a motorized epi-fluorescence microscope (Nikon Ti) equipped with programmable motorized microscope stage (#H117, Prior Scientific) (**Fig. S2**). A pulsed laser (~7 ns pulses @ max. 20 Hz) tuned at a wavelength of 561 nm (Opolette^{TM} HE 355 LD, OPOTEK Inc., Faraday Ave, CA, USA) was applied to illuminate the AuNPs in order to generate VNB. A beam expander (#GBE05-A, Thorlabs) combined with iris diaphragm (#D37SZ, Thorlabs) is used to adjust the laser beam from tens of micrometers to hundreds of micrometers. The setup has time-response and light scattering modes to allow detection of VNB formation as detailed elsewhere (**Fig. S1c**). In order to apply a single laser pulse to a selected region in the cell culture, the stage was synchronized with the pulsed laser by a pulse generator (BNC575, Berkeley Nucleonics Corporation, CA, USA). The microscope xy-translation stage is used to move the sample at the desired location into the photoporation laser beam. In this work we used laser fluence level of 2 J/cm^2 (unless specified otherwise) above the vapour nanobubble threshold (~0.5 J/cm^2 @ 561 nm & 7 ns pulse duration) of the 70 nm AuNP used here. This laser fluence was optimized in previous work of ours.

Pre-defined pattern SNAP. Photoporation of pre-defined patterns was implemented according to a line-scanning procedure and a pixel-based mode. In the line-scanning

ACCEPTED MANUSCRIPT

mode, the xy-translation stage is moved linearly with constant speed between start and end points of subsequent lines (**Fig. S3a**). The laser pulse frequency, laser beam diameter and scanning speed are adjusted so that each location along the line receives a single laser pulse. For example, for a laser beam of 150 µm the pulse frequency is set at 20 Hz with a stage speed of 3 mm/s.

In the pixel-based mode the sample is moved into the photoporation beam according to the pixels of a binary image (**Fig. S3c**). The sample receives a single laser pulse for each indicated pixel location. The image pixel coordinates are transformed to global coordinates by:

$$X_i = (x_i - x_0) \cdot \Delta l + X_0 \quad (1) \qquad Y_i = (y_i - y_0) \cdot \Delta l + Y_0 \quad (2)$$

where x_i, y_i are the coordinates of pixels in the picture, x_0, y_0 are the coordinates of the origin in the image (typically with the top left pixel is chosen as x_0=0, y_0=0), Δl is the image pixel size which is set as 80% diameter of the photoporation laser beam, X_0, Y_0 are the global coordinates of the origin of the microscope stage (i.e. where the top left pixel from the image corresponds to the desired location in the sample).

Image-guided SNAP. Image-guided photoporation was implemented according to a manual and automated mode. In the manual mode, the cells of interest are manually positioned at the center of the microscope's field of view and receive a single laser pulse. Alternatively, the coordinates of the cells of interest can be determined first manually and used as input for subsequent automated photoporation.

In the automated mode, cells in the culture well are first imaged, typically using a low magnification 10× objective (CFI Plan Apochromat, Nikon, Badhoevedorp, The Netherlands). In case the cells cover a large area, multiple adjacent images can be acquired (**Fig. S6**). Dedicated image processing routines can be used to subsequently localize the cells of interest in the recorded images based on morphological features or the presence of a certain (fluorescent) cell marker. The local coordinates of the cells in the images are then transformed to global coordinates of the microscope stage by:

$$X_i^k = (x_i - x_{Laser}) \cdot \Delta l + X^k \quad (3) \qquad Y_i^k = (y_i - y_{Laser}) \cdot \Delta l + Y^k \quad (4)$$

where X_i^k, Y_i^k are the global coordinates of ith cell in k^{th} image, x_i, y_i (in pixel units) are the local coordinates of that cell, x_{Laser}, y_{Laser} (pixel units) are the local coordinates of

ACCEPTED MANUSCRIPT

where the laser beam is centered in the image, Δl is the image pixel size. In this work we used local maxima or minima of the selected cells to define the cell coordinate.

SNAP validation experiments. Pre-defined pattern phtotoporation was validated by SNAP delivery of QDs or fluorescent labeled dextran into HeLa cells cultured in 6-wells plate (~5.0×10^5 cells/well). HeLa cells were obtained from ATCC (CCL-2) and cultured in complete cell medium which consisted of DMEM/F-12 (FBS, Gibco, Invitrogen, Belgium) supplemented with 10% heat-inactivated foetal bovine serum (FBS), 2 mM glutamine and 100 U/mL penicillin/streptomycin (Gibco, Invitrogen, Belgium). Cells were cultured at 37°C in a humid atmosphere containing 5% CO_2. HeLa cells were cultured for 24 hours before laser treatment.

After incubation with AuNPs for 0.5 h, photoporation was performed as described in the main text. Following laser irradiation, the samples were washed a few times with PBS after which new cell medium was added. Next, the cells are put back in the cell incubator for recovery (37°C in humidified atmosphere at 5% CO_2). The cells are finally imaged by confocal microscopy to evaluate the photoporation results.

NHEK cell culture. NHEKs (Normal Human Epidermal Keratinocytes) were purchased from Lonza (#192907, Lonza). NHEKs were cultured in KGM-Gold™ Keratinocyte Growth Medium (KGM-Gold BulletKit, #00192060, Lonza) at 37°C with 5% CO_2 atmosphere. 300,000 cells were seeded in a 100 mm dish (cell density ~3800 cells/cm^2) and subcultured at ~70% confluence. The number of population doublings (PD) was calculated at each passage according to[26]: $PD=log(N_{collected\ cells}/N_{plate\ cells})/log2$.

Toxicity measurement of NHEK cells. NHEKs in the exponential growth phase were plated in 24 well plates (5000 cells/well) 24 h before labeling or photoporation. For Hoechst labeling, the cells were incubated with Hoechst 33342 (2 µg/ml) for 15 min at room temperature. For labeling with Alexa 647-dextran with 10 kDa (AD10), cells were incubated with Alexa dextran at a concentration of 20 µg/ml for 24 h at 37°C. Next, cells were incubated with AuNPs at the indicated concentration for 0.5 h, after which photoporation was performed in the cells in the whole well. The samples were finally

ACCEPTED MANUSCRIPT

washed a few times with PBS and supplemented with new cell medium. After labeling or photoporation, cells were cultured for another 4 days at 37°C and 5% CO_2 atmosphere. MTT cytotoxicity measurements were finally performed. Briefly, 30 µl of a 5 mg/ml 3-(4,5-dimethylthiazol-2-yl)-2,5-diphenyltetrazolium bromide (MTT, Sigma, Belgium) solution is added to each well. Following an incubation period of three hours at 37°C the MTT containing cell medium was removed and cells were lysed using dimethylsulfoxide (Sigma, Belgium). When the formazan crystals were completely dissolved and a homogeneous colour was obtained, the absorbance in each well was measured at 570 and 650 nm using an Envision Xcite multilabel reader (PerkinElmer LAS, Boston, MA).

Cell-selective photoporation and isolation of PK and MK cells. NHEKs in the exponential growth phase were plated in 24 well plates with 5000 cells/well before incubation with AD10. 20 µg/mL of AD was added to the cell medium for 24 h at 37°C and 5% CO_2 to label endolysosomes in the perinuclear area. Next, cells were incubated with AuNPs at the relevant concentrations (see main text) for half an hour, followed by washing with PBS. Cells were finally imaged by confocal microscopy with a low magnification 10× objective. 12 by 12 images were recorded to visualize the entire 24-well plate. The location of MK and PK cells was determined by image processing as described in the main text and **Fig. S9**. With our Matlab code it typically took 5-10 min to process all the images (144 frames). Finally, FD10 was added to the cells for labeling of the selected cells by photoporation. After laser treatment, cells were washed, supplied with fresh cell medium and imaged again before being put back in the incubator for 24 h. The cells were subsequently collected for sorting by BD FACS Aria III (BD Biosciences, Erembodegem, Belgium). Sorting was based on the presence of FITC signal. After sorting, PK/MK cells were collected for further culture and quantification of isolation levels. The isolation level of PK was defined as,

$$P_{PK} = \frac{N_{PK}}{N} \quad (5)$$

where N_{PK} is the number of PK cells and N is the total number of collected cells. Similarly, MK isolation is defined as,

$$P_{MK} = \frac{N_{MK}}{N} \quad (6)$$

ACCEPTED MANUSCRIPT

where N_{MK} is the number of MK cells.

References

[1] R. Strack, Protein labeling in cells, Nature Methods, 13 (2016) 33-33.
[2] Z.Y. Zhang, S.J. Kenny, M. Hauser, W. Li, K. Xu, Ultrahigh-throughput single-molecule spectroscopy and spectrally resolved super-resolution microscopy, Nature Methods, 12 (2015) 935-938.
[3] D.S. D'Astolfo, R.J. Pagliero, A. Pras, W.R. Karthaus, H. Clevers, V. Prasad, R.J. Lebbink, H. Rehmann, N. Geijsen, Efficient Intracellular Delivery of Native Proteins, Cell, 161 (2015) 674-690.
[4] Y.C. Wu, T.H. Wu, D.L. Clemens, B.Y. Lee, X.M. Wen, M.A. Horwitz, M.A. Teitell, P.Y. Chiou, Massively parallel delivery of large cargo into mammalian cells with light pulses, Nature Methods, 12 (2015) 439-+.
[5] A. Erazo-Oliveras, K. Najjar, L. La Dayani, T.Y. Wang, G.A. Johnson, J.P. Pellois, Protein delivery into live cells by incubation with an endosomolytic agent, Nature Methods, 11 (2014) 861-867.
[6] M.P. Stewart, A. Sharei, X. Ding, G. Sahay, R. Langer, K.F. Jensen, In vitro and ex vivo strategies for intracellular delivery, Nature, 538 (2016) 183-192.
[7] K. Dhakal, S. Batabyal, W. Wright, Y.T. Kim, S. Mohanty, Optical delivery of multiple opsin-encoding genes leads to targeted expression and white-light activation, Light-Science & Applications, 4 (2015).
[8] J. Chung, N. Miura, A. Ito, M. Sawada, S. Nishikawa, K. Kuroda, M. Ueda, Single-cell heterogeneity in suppression of PC12 differentiation by direct microinjection of a differentiation inhibitor, U0126, Cell Biology International, 38 (2014) 1215-1220.
[9] K. Remaut, V. Oorschot, K. Braeckmans, J. Klumperman, S.C. De Smedt, Lysosomal capturing of cytoplasmic injected nanoparticles by autophagy: An additional barrier to non-viral gene delivery (vol 195, pg 29, 2014), Journal of Controlled Release, 199 (2015) 179-179.
[10] L.Q. Chang, D. Gallego-Perez, X. Zhao, P. Bertani, Z.G. Yang, C.L. Chiang, V. Malkoc, J.F. Shi, C.K. Sen, L. Odonnell, J.H. Yu, W. Lu, L.J. Lee, Dielectrophoresis-assisted 3D nanoelectroporation for non-viral cell transfection in adoptive immunotherapy, Lab on a Chip, 15 (2015) 3147-3153.
[11] T. Jain, J. Muthuswamy, Bio-chip for spatially controlled transfection of nucleic acid payloads into cells in a culture, Lab Chip, 7 (2007) 1004-1011.
[12] L.E. Barrett, J.Y. Sul, H. Takano, E.J. Van Bockstaele, P.G. Haydon, J.H. Eberwine, Region-directed phototransfection reveals the functional significance of a dendritically synthesized transcription factor, Nature Methods, 3 (2006) 455-460.
[13] U.K. Tirlapur, K. Konig, Cell biology - Targeted transfection by femtosecond laser, Nature, 418 (2002) 290-291.
[14] M. Antkowiak, M.L. Torres-Mapa, E.C. Witts, G.B. Miles, K. Dholakia, F.J. Gunn-Moore, Fast targeted gene transfection and optogenetic modification of single neurons using femtosecond laser irradiation, Scientific Reports, 3 (2013).
[15] R. Xiong, S.K. Samal, J. Demeester, A.G. Skirtach, S.C. De Smedt, K. Braeckmans, Laser-assisted photoporation: fundamentals, technological advances and applications, Advances in Physics: X, (2016) 1-25.
[16] A.G. Skirtach, C. Dejugnat, D. Braun, A.S. Susha, A.L. Rogach, W.J. Parak, H. Mohwald, G.B. Sukhorukov, The role of metal nanoparticles in remote release of encapsulated materials, Nano Letters, 5 (2005) 1371-1377.
[17] R. Xiong, K. Raemdonck, K. Peynshaert, I. Lentacker, I. De Cock, J. Demeester, S.C. De Smedt, A.G. Skirtach, K. Braeckmans, Comparison of Gold Nanoparticle Mediated Photoporation: Vapor Nanobubbles Outperform Direct Heating for Delivering Macromolecules in Live Cells, ACS Nano, 8 (2014) 6288-6296.
[18] E.Y. Lukianova-Hleb, D.S. Wagner, M.K. Brenner, D.O. Lapotko, Cell-specific transmembrane injection of molecular cargo with gold nanoparticle-generated transient plasmonic nanobubbles, Biomaterials, 33 (2012) 5441-5450.
[19] R. Xiong, F. Joris, S. Liang, R. De Rycke, S. Lippens, J. Demeester, A. Skirtach, K. Raemdonck, U. Himmelreich, S.C. De Smedt, K. Braeckmans, Cytosolic Delivery of Nanolabels Prevents Their Asymmetric Inheritance and Enables Extended Quantitative in Vivo Cell Imaging, Nano Letters, (2016).

ACCEPTED MANUSCRIPT

[20] N. Saklayen, M. Huber, M. Madrid, V. Nuzzo, D.I. Vulis, W. Shen, J. Nelson, A.A. McClelland, A. Heisterkamp, E. Mazur, Intracellular Delivery Using Nanosecond-Laser Excitation of Large-Area Plasmonic Substrates, Acs Nano, 11 (2017) 3671-3680.
[21] M. Schomaker, D. Heinemann, S. Kalies, S. Willenbrock, S. Wagner, I. Nolte, T. Ripken, H.M. Escobar, H. Meyer, A. Heisterkamp, Characterization of nanoparticle mediated laser transfection by femtosecond laser pulses for applications in molecular medicine, Journal of Nanobiotechnology, 13 (2015).
[22] K. Gosselin, S. Martien, A. Pourtier, C. Vercamer, P. Ostoich, L. Morat, L. Sabatier, L. Duprez, C.T. de Roodenbeke, E. Gilson, N. Malaquin, N. Wernert, P. Slijepcevic, M. Ashtari, F. Chelli, E. Deruy, B. Vandenbunder, Y. De Launoit, C. Abbadie, Senescence-Associated Oxidative DNA Damage Promotes the Generation of Neoplastic Cells, Cancer Research, 69 (2009) 7917-7925.
[23] J. Nassour, S. Martien, N. Martin, E. Deruy, E. Tomellini, N. Malaquin, F. Bouali, L. Sabatier, N. Wernert, S. Pinte, E. Gilson, A. Pourtier, O. Pluquet, C. Abbadie, Defective DNA single-strand break repair is responsible for senescence and neoplastic escape of epithelial cells, Nature Communications, 7 (2016) 10399.
[24] G.C. Messina, M. Dipalo, R. La Rocca, P. Zilio, V. Caprettini, R.P. Zaccaria, A. Toma, F. Tantussi, L. Berdondini, F. De Angelis, Spatially, Temporally, and Quantitatively Controlled Delivery of Broad Range of Molecules into Selected Cells through Plasmonic Nanotubes, Advanced Materials, 27 (2015) 7145-+.
[25] C.A. DeForest, D.A. Tirrell, A photoreversible protein-patterning approach for guiding stem cell fate in three-dimensional gels, Nature Materials, 14 (2015) 523-531.
[26] E. Deruy, J. Nassour, N. Martin, C. Vercamer, N. Malaquin, J. Bertout, F. Chelli, A. Pourtier, O. Pluquet, C. Abbadie, Level of macroautophagy drives senescent keratinocytes into cell death or neoplastic evasion, Cell Death & Disease, 5 (2014).

ACCEPTED MANUSCRIPT

ACCEPTED MANUSCRIPT

Acknowledgments

Financial support by the Ghent University Special Research Fund is acknowledged with gratitude by KB and AGS. RX gratefully acknowledges the financial support from China Scholarship Council (CSC). CD was supported by a fellowship "Accueil jeune chercheur" from Région Nord-Pas-de-Calais. KB and AGS would like to acknowledge the Research Foundation Flanders (FWO Vlaanderen). KB acknowledges financial support from the European Research Council (ERC) under the European Union's Horizon 2020 research and innovation program (grant agreement No 648124). AGS acknowledges ERA-Net Rus project "Intelbiocomp" for support. CA acknowledges financial support from Ligue contre le cancer, from SIRIC OncoLille (grant INCa-DGOS-Inserm 6041) and from the joint call Ghent-Lille-UCLouvain.

Competing interests: The authors declare no competing financial interests.

ACCEPTED MANUSCRIPT

ACCEPTED MANUSCRIPT

Graphical abstract